# APPENDIX A

## In-ice Calibration Tests for an Elongated, Uniaxial Brass Ice Stress Sensor

J.B. Johnson
US Army Cold Regions Research and
Engineering Laboratory

(In, Proc. of the Fourth International Offshore Mechanics and Arctic Engineering Symposium, February 17-21, 1985, Dallas, TX.)

# IN-ICE CALIBRATION TESTS FOR AN ELONGATED, UNIAXIAL BRASS ICE STRESS SENSOR

Jerome B. Johnson
U.S. Army Cold Regions Research and
Engineering Laboratory
Hanover, NH

## ABSTRACT

An elongated, uniaxial brass ice stress sensor has been developed by the University of Alaska and used in several field experiments. Laboratory calibration tests have been conducted, in a 60 x 29.5 x 8.5 in. (1524 x 750 x 216 mm) ice block into which the sensor was frozen, to determine the sensor's response characteristics. Test results indicate that the sensor acts as a stress concentrator with a stress concentration factor of 2.4 and transverse sensitivity of -1.3 at stresses below 30 lbf/in.$^2$ (207 kPa). At stresses greater than 30 lbf/in.$^2$ (207 kPa) the stress concentration factor increased and the sensor exhibited a time delay response to load. Differences of 22% were measured between the measured sensor stress immediately after a constant ice load was applied and the asymptotic stress limit. Interpretation of measured sensor stresses can be considered reliable at ambient ice stress levels below 30 lbf/in.$^2$ (207 kPa).

## INTRODUCTION

Ice stress is recognized as an important factor in the design of marine and hydraulic structures, ice drift, ride-up, pile-up, pressure ridge formation and pressures in reservoirs. Cox and Johnson [1] reviewed the design and response characteristics of several sensors that have been built to measure stresses in an ice sheet.

One of the early stress sensor designs was developed at the University of Alaska. Nelson [2] and Nelson et al. [3] described the design requirements and experimental test results for an elongated, uniaxial brass ice stress sensor. The sensor was constructed from a brass bar with a reduced diameter section. Strain gauges are attached to the reduced diameter section such that all arms of the strain bridge are active. A copper sheathing covering and a waterproofing compound protect the electronics. End-caps extend from the ends of the transducer to provide tension gripping in the ice (Fig. 1). The initial development and calibration of the sensor was conducted using a 3 in. (76 mm) long by 1 in. (25.4 mm) diameter gauge with a 1 in. (25.4 mm) reduced diameter section 2-1/2 in. (63.5 mm) in length [3].

Direct load calibration tests were conducted by Nelson et al. [3] and included creep loading, rapid loading, and loading until the ice block failed. These tests indicated that the stress concentration factors varied from 3.4 to 6.4 depending on the type of test conducted. The stress concentration factor, $\alpha$, is defined as the ratio of the measured stress to the applied stress when the long axis of the sensor is oriented in the loading direction. These tests also demonstrated that the sensor was sensitive to loads applied perpendicular to the long axis. This transverse sensitivity varied between -1.53 and -0.082, depending on loading conditions. The transverse sensitivity, $\beta$, is defined as the ratio of the measured stress to the applied stress when the long axis of the sensor is oriented normal to the loading direction.

The uniaxial stress sensor has been used in several field experiments to estimate ice stresses near grounded objects, thermal and tide-generated stresses in shorefast sea ice, and stresses associated with ice movement and deformation [4,5,6]. These studies utilized 5 in. (127 mm) long by 2 in. (50.8 mm) diameter sensors as shown in Figure 1. Stress sensor measurements were interpreted by assuming a constant stress concentration factor, $\alpha$, equal to 3.2 and ignoring the transverse sensitivity ($\beta = 0$). The uniaxial sensor has also been used to measure ice

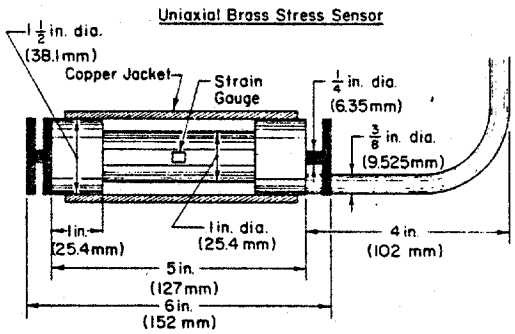


FIG. 1. Elongated, uniaxial brass ice stress sensor.

stresses around offshore structures off the north coast of Canada and Alaska in 1983 and near the coast of Finland in 1984 (Sackinger, personal communication). Past and current interest in utilizing the uniaxial brass stress sensor to measure ice stress points out the need to define the sensor's response characteristics, which have not been well defined or fully utilized. Calibration test results by Nelson et al. [3] showed that $\alpha$ and $\beta$ varied significantly, even when loading test conditions were similar. In addition, analytical analyses of an elongated inclusion inserted into an elastic plate indicate that the stress concentration factor for the uniaxial stress sensor may depend on $\theta$, the angle between the principal stress axis and the long axis of the gauge [7]. Past field experiments using the uniaxial sensor have used data reduction techniques that have ignored the transverse sensitivity of the gauge. These stress measurements may be suspect unless the contribution of transverse sensitivity is negligible.

The present paper presents the results of a calibration test program that was designed to resolve some of the questions raised above about the uniaxial sensor's response to applied loads. The procedure was to: 1) determine experimentally the sensitivity of the uniaxial sensor (change in sensor electrical output per unit change in applied load) before it was embedded in an ice block; 2) determine experimentally the in-ice stress concentration factor of the sensor as a function of $\theta$; 3) determine experimentally the in-ice transverse sensitivity of the sensor; and 4) present an analytical technique for interpreting the in-ice stress sensor calibration results.

## TEST PRODCEDURES

Calibration tests were conducted using a uniaxial sensor with dimensions identical to the sensors that were used in earlier field experiments (Fig. 1). The two basic tests that were conducted included a direct load test on the sensor and loading an ice block into which a sensor had been frozen. The direct load test was conducted by placing weights on one of the endplates of the sensor while the other endplate was held in a vise. The load was cycled several times in an effort to determine the stress sensor's sensitivity, linearity, and hysteresis characteristics. The second test was conducted by freezing the uniaxial sensor into a large freshwater ice block, which was then uniaxially loaded by a hydraulic ram. The ice block was 60 in. long, 29.5 in. wide, and 8 in. thick (1524 x 750 x 216 mm) (Fig. 2). These dimensions were chosen so that the stress disturbance in the ice block due to the presence of the sensor was not felt at the boundaries of the block. The use of an ice block of sufficiently large dimensions is necessary to ensure that the block can adequately represent an infinite ice sheet and thereby reduce the variability of the test results. Nelson et al. [3] used an 8 x 8 x 12 in. (203 x 203 x 304 mm) block for their tests on a 3 x 1 in. (76 x 25 mm) diameter gauge. This small block size may account for some of the variability of their results.

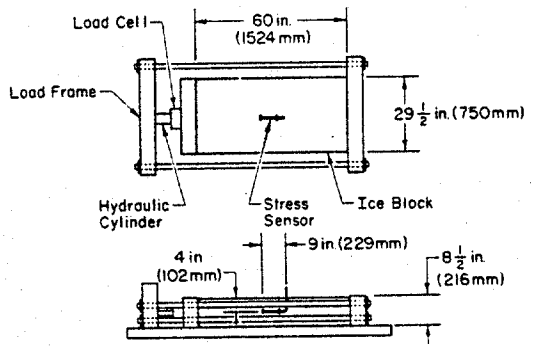


FIG. 2. Experimental test setup for the load frame, ice block, and stress sensor.

Freshwater ice was used for convenience; however, the results should be applicable to saline ice as well. The uniaxial stress sensor was designed to be stiff as compared to ice (i.e. to have an elastic modulus much greater than that of freshwater or saline ice). Nelson [2] has shown analytically that the stress concentration factor of a stiff elongated stress sensor is little affected by changes in the modulus or by creep of the ice. These results are supported by experiments on stiff cylindrical stress sensors which were embedded in both freshwater and saline ice [1,8]. The experiments indicate that differences in the elastic modulus and creep behavior for freshwater and saline ice do not significantly affect the behavior of a stiff stress sensor.

The freshwater ice block used in this experiment was grown in the loading frame (Fig. 2). The base of the frame consisted of a 1 in. (25.4 mm) thick sheet of plywood that was covered with a double layer of plastic sheeting. The plastic sheeting provided a watertight membrane during freezing and a low friction surface under the ice block during loading. The sidewalls of the ice growing frame were also made from plywood. The plywood was coated with a lubricating grease to prevent the ice from bonding during ice growth. The loading platens at the ends of the load frame were covered with a double layer of plastic sheeting. The uniaxial sensor was placed at mid-depth in the center of the framework and allowed to freeze in place. Once the ice block was made, the plywood sidewall supports were removed. The ice block was then loaded using a 100,000 lbf (45 MN) hydraulic cylinder. The loads were monitored with a 150,000 lbf (67 MN) load cell that was mounted in series with the hydraulic cylinder. The load cell was calibrated by the manufacturer and was found to respond linearly over the full range of loads used in the calibration test. Loads were accurately resolved to 150 lbf (670 N) which corresponds to a stress of 0.6 lbf/in.$^2$ (4 kPa). Initially it was planned to run all loading experiments to a maximum stress of 100 lbf/in.$^2$ (689 kPa). As preliminary tests resulted in a shear failure between the loading platens, the maximum stress was limited to 30 lbf/in.$^2$ (207 kPa) for the majority of tests. The applied stress was increased to 70 lbf/in.$^2$ (483 kPa) for the final test series with the sensor's long axis aligned parallel to the direction of the applied stress, $\theta = 0°$.

Tests were conducted at an ice block temperature of 23°F (-5°C) with the sensor at five different orientations to the applied stress. The sensor was first tested at $\theta = 0°$. A chain saw was used to remove the sensor from the ice. The sensor was then reoriented to $\theta = 30°$ and refrozen into the center of the block, and another set of tests were conducted. This procedure was repeated for $\theta = 45°$, 60°, and 90°. There was some concern that removing the sensor from the ice block and then refreezing it into the block might alter the test conditions. The effect of the removal/installation process was examined by conducting the final test series by removing the gauge after

the $\theta = 90°$ test and refreezing it at $\theta = 0°$. The results of the last test series were then compared with those of the first test with $\theta = 0°$ and found to be the same within the limits of experimental error.

Both rapid-loading and creep tests were conducted on the ice block into which the sensor was embedded. The rapid-loading tests were performed by increasing and then decreasing the load incrementally. The load was allowed to stabilize briefly before being changed. Creep tests were conducted by increasing the applied load to a given level and maintaining it until the stress sensor response was stable.

The excitation voltage for the strain gauge bridge mounted on the sensor was set at 6 V. This is the same level that has been used in all past field experiments. The load information from the load cell and stress sensor were recorded on an x-y plotter. The data presented here are based on the x-y plotter records.

## DATA REDUCTION AND TEST RESULTS

Stress sensor load sensitivity was determined from the direct loading test. These results indicate that the sensor response is repeatable, linear and had little hysteresis (Fig. 3). The load sensitivity for these tests was given by

$$\Delta F = G\ S\ E_0 = (1.27\ \text{lb}/\mu\text{V})\ E_0$$

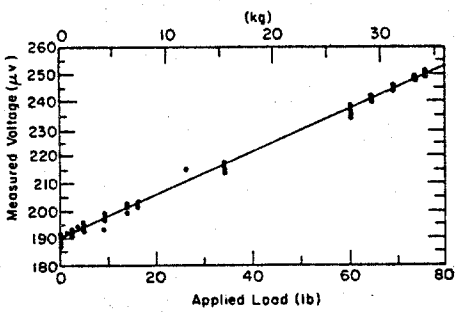


FIG. 3. Load sensitivity for the uniaxial brass ice stress sensor from direct loading tests.

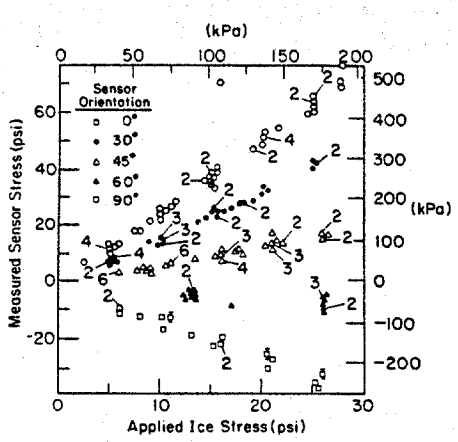


FIG. 4. Results of low-magnitude stress-loading tests in ice. The number of separate measurements taken at a given applied stress are shown in the figure.

Table 1. Summary of Statistics on Calibration Data.

| Stress sensor orientation to loading (deg) | Least Squares Fit to Data: Correlation coefficient | Slope | Vertical axis intercept | Standard deviation about the slope* |
|---|---|---|---|---|
| 0 | 0.95 | 2.4 | 2.1 | 0.1 |
| 30 | 0.99 | 1.7 | -1.8 | 0.2 |
| 45 | 0.99 | 0.7 | -0.9 | 0.1 |
| 60 | -0.58 | -0.2 | -2.0 | 0.1 |
| 90 | -0.98 | -1.3 | -1.6 | 0.2 |

* The slope is also the mean ratio of measured sensor stress and applied ice stress.

where $\Delta F$ is the change in load, G is the amplification gain, S is the load sensitivity coefficient, and $E_0$ is the sensor output in volts. Measured stresses were determined by dividing the load sensitivity of the sensor by the surface area of the endcaps:

$$\sigma_m = \Delta F/A\ .$$

Applied ice block stresses were determined by dividing the measured load from the load cell by the cross sectional area of the ice block. The test results are presented in four different formats to illustrate the behavior characteristics of the sensor. The original test results for stress sensor orientations of 0°, 30°, 45°, 60°, and 90° to the principal stress direction are shown in Figure 4. A linear least squares method was used to fit a line to each of the data sets shown in Figure 4. The coefficients determined from the least squares fit are presented in Table 1. The slope of the fitted line is also the mean value of the ratio of measured sensor stress to applied ice block stress. The slope of the fitted curve for $\theta = 0°$ is the mean stress concentration factor; it was found to be 2.4 with a standard deviation of 0.1. The mean transverse sensitivity of the sensor was determined from the slope of the fitted curve at $\theta = 90°$ and was -1.3 with a standard deviation of 0.2.

The results shown in Figure 4 indicate that the sensor response was generally linear in each orientation. However, the magnitude of the applied stress that was detected by the sensor did depend on orientation. This behavior was expected since the sensor was designed to sense stresses along its axis, and these would vary depending on the orientation of the sensor to the applied load. Nelson et al. [3] suggested that the measured sensor stress could be related to the applied stress by a Mohr's circle representation. For a uniaxial stress field, the ratio of measured stress, $\sigma_m$, to applied stress, $\sigma_a$, can be given by

$$\sigma_m/\sigma_a = (\alpha \cos^2\theta + \beta \sin^2\theta)\ . \qquad (1)$$

Figure 5 is a plot of the mean value of $\sigma_m/\sigma_a$ for each test orientation. The standard deviation about the mean is delineated by the bars extending from the data points. The calculated curve for $\sigma_m/\sigma_a$ is also plotted:

$$\sigma_m/\sigma_a = 2.4 \cos^2\theta - 1.3 \sin^2\theta$$

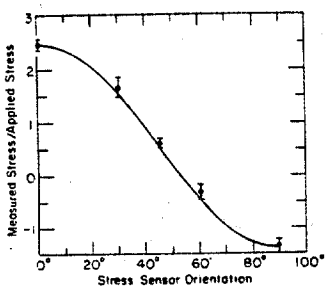


FIG. 5. Measured sensor stress to applied ice-stress ratio as a function of stress sensor orientation to the principal stress direction.

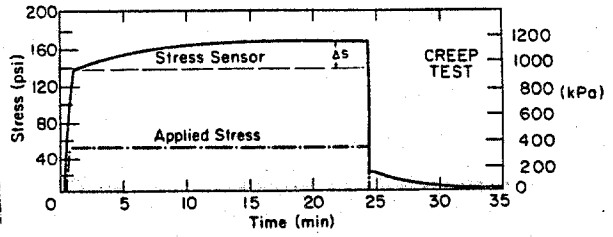


FIG. 6. Creep loading test results. The difference between the initial measured stress after imposing a constant applied stress and the asymptotic limit of the measured stress is shown by ΔS.

where the stress concentration factor at 0° is 2.4 and the tangential sensitivity of the sensor at 90° is -1.3. The calculated results agree with equation 1, supporting Nelson's suggestion that the measured stress/applied stress ratio can be represented by the Mohr circle theory.

The typical response of the uniaxial ice stress sensor to a constant load as a function of time is shown in Figure 6. Here the measured sensor stress increases as the applied ice stress is increased to a constant 50 lbf/in.$^2$ (346 kPa) magnitude. The measured stress then continues to increase asymptotically to a limiting value as the time increases. The difference between the measured sensor stress immediately after the applied stress reached a constant value and the asymptotic limit of the measured sensor stress was 22% (ΔS in Fig. 6). The sensor did not exhibit a time-dependent response to load during the direct loading test. This indicates that the time response of the sensor in ice must be due to the interaction of ice and sensor. The sensor configuration may produce its time-dependent response in ice to creep loading. The endcaps of the sensor are designed so that ice will form around them, allowing the sensor to respond to both compressive and tensile stresses. The ice that fills the region between the backside of the endplates and the body of the sensor may support some of the applied ice stress through shear to the main ice sheet. As the applied load is maintained, the ice plug may begin to creep, allowing the sensor to gradually assume the full load due to the applied ice stress. Test results indicate that the sensor's time-dependent response to creep loading is more severe at higher applied stresses.

A final test was performed at $\theta = 0°$ to examine the relationship between the stress concentration factor and the magnitude of the applied stress. This was the only test sequence that was conducted at stress levels greater than 30 lbf/in.$^2$ (207 kPa). At these higher stress levels, noticeable cracking of the ice near the loading platens was observed. Eventually, cracks formed in the body of the block, and the test was ended. The test results indicated that the stress concentration factors were scattered in a range that was consistent with $\alpha = 2.4$ when the applied ice stress was 30 lbf/in.$^2$ (207 kPa) or less. At stress levels between 30 lbf/in.$^2$ (207 kPa) and 70 lbf/in.$^2$ (483 kPa) the stress concentration factors increased to more than 3 (Fig. 7). The larger stress concentration factors at higher loads may be due to local ice cracking around the sensor, which resulted in increased load transfer to the sensor. Too few tests were conducted to fully document the relationship between the stress concentration factor and applied stress. However, the available results are generally consistent with the findings of Nelson et al. [3] and indicate that different α values should be used to interpret measured stresses correctly, depending on the loading conditions and stress magnitude (for example, rapid loading, creep loading, or loading to ice block failure).

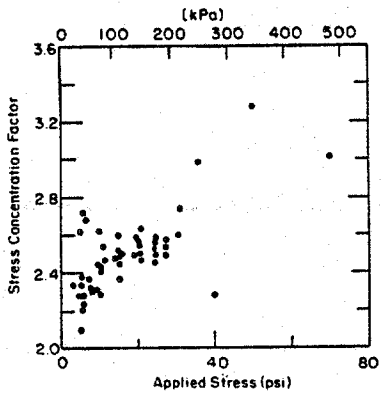


FIG. 7. Stress concentration factor as a function of the applied ice stress for $\theta = 0°$ configuration.

## IMPLICATION OF CALIBRATION TEST RESULTS ON DATA INTERPRETATION

The calibration test results described in the previous section indicate that at applied ice stresses below 30 lbf/in.$^2$ (207 kPa), the measured stresses can be reasonably described by using a Mohr's circle representation of the sensor response and constant values for α and β. At stress levels above 30 lbf/in.$^2$ (207 kPa) the time-dependent response characteristics and the dependence of α on the applied ice stress of the uniaxial stress sensor become important.

For relatively low ambient ice-stress levels, the Mohr circle representation suggested by Nelson et al. [3] can be used to interpret field data. The measured ice stresses can be related to the principal stresses in a biaxial stress field by

$$\sigma_m = (\alpha+\beta)\frac{p_1+p_2}{2} + (\alpha-\beta)\frac{p_1-p_2}{2}\cos 2\theta$$

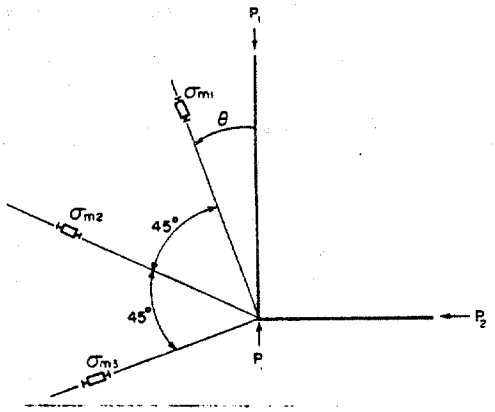


FIG. 8. Stress sensor rosette used to determine the magnitude and direction of the principal stresses.

where $p_1$ and $p_2$ are the primary and secondary principal stresses acting on an ice sheet. The principal stresses $p_1$ and $p_2$ acting on an ice sheet can be determined by using a rosette of three stress sensors embedded in the ice. If the sensors have an angular separation of 45° as shown in Figure 8, then

$$p_1 = \frac{\sigma_{m_1} + \sigma_{m_3}}{2(\alpha+\beta)} + \frac{\left[(\sigma_{m_1} - 2\sigma_{m_2} + \sigma_{m_3})^2 + (\sigma_{m_1} - \sigma_{m_3})^2\right]^{1/2}}{2(\alpha-\beta)}$$

$$p_2 = \frac{\sigma_{m_1} + \sigma_{m_3}}{2(\alpha+\beta)} - \frac{\left[(\sigma_{m_1} - 2\sigma_{m_2} + \sigma_{m_3})^2 + (\sigma_{m_1} - \sigma_{m_3})^2\right]^{1/2}}{2(\alpha-\beta)}$$

$$\tan 2\theta = \frac{\sigma_{m_1} - 2\sigma_{m_2} + \sigma_{m_3}}{\sigma_{m_1} - \sigma_{m_3}}$$

In previous field experiments ice stresses have been calculated without considering the effects of the sensor's transverse sensitivity. The calculated angle of orientation, θ, will not be affected since β does not enter into the formula. The calculated $p_1$ and $p_2$ values may, however, be in error. The errors for $p_1$ and $p_2$ in a biaxial stress field can be derived from the above equations and are given by

$$\Delta p_1 = -\frac{\beta}{\alpha} p_2 \quad \text{and} \quad \Delta p_2 = -\frac{\beta}{\alpha} p_1$$

where $\Delta p_1 = (p_1)_{\alpha,\beta} - (p_1)_{\alpha,0}$ and $\Delta p_2 = (p_2)_{\alpha,\beta} - (p_2)_{\alpha,0}$. $\Delta p_1$ and $\Delta p_2$ are the differences between the calculated principal stresses, assuming the influence of both α and β, and the calculated principal stresses, assuming no transverse sensitivity. For $\alpha = 2.4$ and $\beta = -1.3$, as were determined from the calibration tests, we have

$$\Delta p_1 = 0.52\, p_2 \quad \text{and} \quad \Delta p_2 = 0.52\, p_1.$$

The percentage error is determined by dividing by the principal stresses where

$$\frac{\Delta p_1}{p_1} = 0.52\, \frac{p_2}{p_1} \quad \text{and} \quad \frac{\Delta p_2}{p_2} = 0.52\, \frac{p_1}{p_2}.$$

These results show that the errors associated with setting $\beta = 0$ depend on the biaxial stress ratios $p_2/p_1$ and $p_1/p_2$ and can be significant. The calculated stresses can differ up to 52% from actual ice stresses by assuming $\beta = 0$. This indicates that the transverse sensitivity factor should be taken into account in all calculations where the direction and magnitudes of the principal stresses are not known. The errors associated with assuming $\beta = 0$ can be reduced or eliminated in special situations when the secondary principal stress, $p_2$, is known to be negligible.

Interpretation of measured sensor stress becomes difficult at higher stress magnitudes because of a variation of stress concentration factor with applied stress. Additional calibration tests need to be conducted to better define the applied ice-stress/stress concentration factor relationship and determine if it is repeatable. If the increase in the stress concentration factor is due to local fracturing around the sensor it is doubtful that any applied ice-stress/stress concentration factor relationship will be repeatable. However, one possible method of interpreting measured stresses would be to calculate ice stress using the low stress level α. The calculated stress magnitude could then be used to estimate the appropriate α value to be used in estimating the final stress magnitudes. This is not a very satisfactory method of determining in-situ stresses, and the calibration test results indicate that measured sensor stresses should be viewed with caution when the applied ice stresses are greater than 30 lbf/in.$^2$ (207 kPa).

## CONCLUSIONS

The elongated, uniaxial brass ice stress sensor does respond to low-level ice stresses in a predictable manner. The calibration tests conducted in this study indicate that, for ice stresses less than 30 lbf/in.$^2$ (207 kPa), the ice stress sensor exhibits a stress concentration factor of 2.4 and transverse sensitivity factor of -1.3. The ratio of the measured stress and applied stress can also be described by a Mohr circle representation. The stress concentration factor was found to increase with increasing ice stress for applied stresses in excess of 30 lbf/in.$^2$ (207 kPa). This behavior was attributed to localized ice failure near the sensor. Additional loading tests are required to better define the relationship between stress concentration factor and applied stress. The sensor also exhibited a time-delayed response to constant applied stresses greater than 50 lbf/in.$^2$ (347 kPa). Time delays of up to 20 min. were required for measured sensor stresses to asymptotically approach a stable value after the application of a constant ice stress.

Field experiments utilizing the uniaxial sensor need to be carefully designed to ensure that the ice-stress magnitudes do not exceed the levels at which measured sensor stresses can be confidently calculated. The calibration test results indicate this upper limit of ice stress to be 30 lbf/in.$^2$ (207 kPa). Past field experiments have used a stress concentration factor of 3.2 and have ignored the transverse sensitivity when calculating ice stresses. The stress concentration factor determined in this study is believed to be more reliable than the 3.2 value since earlier experiments were conducted using smaller stress sensors and the test ice-block dimensions were

too small to incorporate the stress disturbance due to the embedded sensor. The earlier experiments showed greater variability in results than was obtained in this study. Calculated ice-stress magnitudes may have significant errors when the effects of transverse sensitivity are not accounted for. The magnitude of these errors depends on the stress concentration/ transverse sensitivity ratio for the sensor and the ratio of primary to secondary principal stress. The calibration tests indicate that errors of up to 52% may occur for the uniaxial sensor, when the transverse sensitivity of the sensor is not included in the analysis of measured stresses.

ACKNOWLEDGMENT

This work was supported by the Minerals Management Service, U.S. Department of the Interior. I express my appreciation to Dr. William M. Sackinger for his encouragement and support while conducting this study, to Mr. Dan Solie for assisting with the experiments and to Dr. Gordon F.N. Cox and Dr. Devinder S. Sodhi for technically reviewing the report.

REFERENCES

1. Cox, G.F.N. and Johnson, J.B. Stress Measurements in Ice, U.S. Army Cold Regions Research and Engineering Laboratory, CRREL Report 83-23, Hanover, N.H., 1983, 31 pp.

2. Nelson, R.D. Internal Stress Measurements in Ice Sheets Using Embedded Load Cells, in Proceedings of the 3rd International Conference on Port and Ocean Engineering Under Arctic Conditions: University of Alaska, Fairbanks, Vol. 1, 1975, pp. 361-373.

3. Nelson, R.D., Tauriainen, M. and Borghorst, J. Techniques for Measuring Stress in Sea Ice, University of Alaska, Alaska Sea Grant Report No. 77-1, 1977, 65 pp.

4. Nelson, R.D. Measurement of Tide and Temperature-Generated Stresses in Shorefast Sea Ice, in The Coast and Shelf of the Beaufort Sea (J.C. Reed and J.C. Slater, eds.), Arctic Institute of North America, 1974, pp. 195-204.

5. Rogers, J.C., Sackinger, W.M. and Nelson, R.D. Arctic Coastal Sea Ice Dynamics, in Proceedings of the Offshore Technology Conference, May 6-8, Houston, Texas, Vol. 2, paper No. 2047, 1974, p p. 133-144.

6. Sackinger, W.M. and Nelson, R.D. Measurements of Sea-Ice Stresses Near Grounded Obstacles, Journal of Energy Resources Technology, Vol. 102, no. 3, 1980, pp. 144-147.

7. Savin, G.N. Stress Concentrations around Holes: New York, Pergamon Press, 1961, 430 pp.

8. Johnson, J.B. and Cox, G.F.N. The OSI Ice Stress Sensor, In Proceedings of the Workshop on Sea Ice Field Measurements, St. John's, Newfoundland. Center for Cold Oceans Resources Engineering, C-CORE Report 80-21, 1980, pp. 193-207.